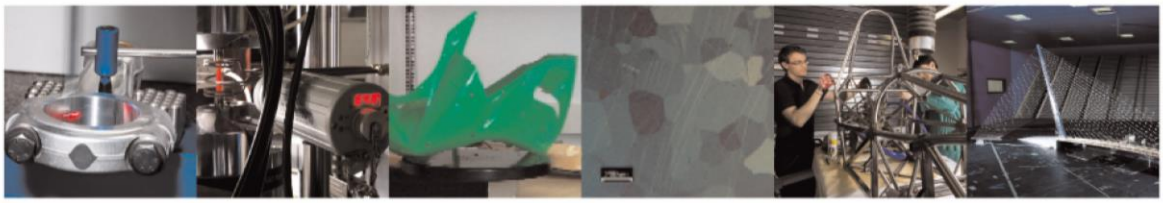

Direct laser interference patterning via scanning optics using the Michelson-Morley configuration

Valentina Furlan, Ali Gokhan Demir, Andrea Bianco

This is a post-peer-review, pre-copyedit version of an article published in Applied Surface Science. The final authenticated version is available online at:
http://dx.doi.org/10.1016/j.apsusc.2022.154536

DIPARTIMENTO DI MECCANICA ■ POLITECNICO DI MILANO
via G. La Masa, 1 ■ 20156 Milano ■ EMAIL (PEC): pecmecc@cert.polimi.it
http://www.mecc.polimi.it
Rev. 0

Direct Laser Interference Patterning via scanning optics using the Michelson-Morley configuration

Valentina Furlan[1*], valentina.furlan@polimi.it
Ali Gökhan Demir[1], aligokhan.demir@polimi.it
Andrea Bianco[2], andrea.bianco@brera.inaf.it

[1] Department of Mechanical Engineering, Politecnico di Milano, Via La Masa 1, 20156 Milan, Italy
[2] INAF – Osservatorio Astronomico di Brera, Via E. Bianchi 46, 23807 Merate, Lecco, Italy
*Corresponding author

Direct Laser Interference Patterning via scanning optics using the Michelson-Morley configuration

Valentina Furlan[1*], valentina.furlan@polimi.it

Ali Gökhan Demir[1], aligokhan.demir@polimi.it

Andrea Bianco[2], andrea.bianco@brera.inaf.it

[1]Department of Mechanical Engineering, Politecnico di Milano, Via La Masa 1, 20156 Milan, Italy

[2]INAF – Osservatorio Astronomico di Brera, Via E. Bianchi, 46, 23807 Merate, LC, Italy

*Corresponding author

Abstract

Direct Laser Interference Patterning (DLIP) is a promising method to realize patterns on surfaces, based on two or more beams interference. Compared with the traditional direct laser writing approach, DLIP allows control of the features' shape and size. The standard configuration of a DLIP system is based on fixed optical elements and the movement of the sample via a motorized axis. This work proposes a new optical setup for two-beam DLIP. A Michelson-Morley interferometer was used, realizing the interference of a split beam. A nanosecond pulsed green laser was used to realize the interference phenomenon. The innovative concept combines the interferometer with an industrial scanner head for beam steering. The work explores possibility to use the galvanometric mirrors in DLIP to expand the process capabilities towards larger areas without moving the workpiece. Moreover, the concept is adaptable for different laser wavelengths and optical solutions permitting a degree of flexibility in the pattern period. An optical model is proposed for the first time to describe the design requirements and the pattern period for scanning optics. The developed prototype was used to pattern a biodegradable magnesium alloy with known difficulties for nanosecond pulse ablation. Two strategies namely point by point and continuous scanning were investigated. Periodic linear patter were produced with periodicity equal to 23 μm and with a productivity up to 6.5 cm^2/min.

Keywords: laser surface texturing; Michelson-Morley interferometry; optical modeling; biodegradable metals; green pulsed laser.

1 Introduction

Micro, sub-micro, nano patterns and their hierarchical combinations attract growing interest for several applications. In these patterns morphology describe features shapes and feature distribution, while topography quantify features characteristics. A greater control over the surface patterns allows to tailor the surface functions in a flexible manner. For instance, such patterns can be used to reduce friction and wear in mechanical components [1],[2]. Surface patterns can be used to manipulate the adhesion of a coating on a substrate for aerospace or biomedical devices [3],[4]. They can be used to modify optical properties of the surfaces for solar cells and display applications [5],[6]. In a similar manner, such surface patterns can play a crucial role in antibacterial properties as much as in the adhesion and proliferation of cells [1],[2],[4]. In the past years, several patterning techniques were developed, based on different tool-material interactions based on mechanical, chemical, thermal, and ablation-based processes [9]–[15]. Laser based texturing and patterning processes have emerged amongst different processes owing to their flexibility and sustainability in terms of economic and ecologic constrains. Arguably, the most widely used laser based patterning technique is Direct Laser Writing (DLW), where a diffraction limited laser beam patterns the surface by ablation. Inherently, DLW presents several limits on pattern resolution that remains similar to the beam size in the order of a tens of micrometers. For application fields requiring sub-micron to nanometric resolution such processes may not be suitable. One of the approaches to overcome the limits is the use of ultrashort pulsed laser sources (ps and fs). Ultrashort pulsed laser sources can produce laser-induced periodic surface structures (LIPSS), that are commonly in sub-micrometric and nanometric range dimension as pattern period [16],[17],[18]. LIPSS can be applied to different materials, based on the interference between the incident beam and the surface with different mechanisms. Nevertheless, LIPSS does not permit a simple change of pattern period and pattern morphology. Moreover, the overlap of patterns produced by LIPSS is not precise and homogeneous, affecting the continuity of the surface and the possible applications. A promising option is Direct Laser Interference Patterning (DLIP). DLIP is a patterning technique based on laser energy redistribution of the beam spot. In DLIP the combination of two or more beams produces regions of constructive and destructive interference lowering the feature size to dimensions below the spot size. The number of interference beams controls the pattern shape, while the laser wavelength and the interference angle control the pattern period [2],[5],[16]. DLIP can be adopted with different pulsed laser sources [20],[21] moreover the reduction of pulse duration increases the difficulty in making interference.

DLIP works generate multiple periodic structures contemporarily within the single irradiated area potentially increasing the process productivity. In micrometric pattern dimensions, DLIP can be used as a means for parallel machining. In literature, DLIP was studied on various materials [22]–[27] and application fields [24], [28]–[33]. Nevertheless, it is interesting to note that the use of DLIP, for large-area fabrication, is generally carried out with the same set-up that foresees the use of motorized axes, in which the interfered beams are conveniently fixed at a given position and the workpiece is moved [34],[35]–[37]. Such approach ensures the beam stability, while for processing larger areas the system dynamics can be limited to the manipulation of the mechanical axes. In laser ablation processes such as DLW scanner heads are commonly used, where rapid beam manipulation is achieved via the rotational movement of the galvanometric mirrors. The combination of DLIP with scanning optics can indeed open up to several possibilities in terms of improved productivity and applicability to large areas without relative movement between the workpiece and the process head. Such a solution requires the resolution of the beam interference prior to the scanning head and the maintenance of interference on the workpiece [38],[39],[20]. Evidently the literature lacks a complete work that defines the design criteria, the optical modelling approach, and process development for scanner based DLIP.

Accordingly, a new DLIP concept using scanning optics is proposed employing a Michelson-Morley interferometer, an industrial scanner head, and a pulsed green laser source. The work details the design requirements and the optical modelling tools that provide the means for splitting and

overlapping two beams prior to their launch into the scanner head. The same model allows to adapt the system as a function of the laser wavelength and focal distances, which are essential for the feature sizes achievable. Using the design criteria a system has been integrated with a ns-pulsed green diode pumped solid state (DPSS) laser to achieve pattern periodicity at micrometric level suited for parallel machining. The DLIP process has been developed on biodegradable Mg alloy destined to cardiovascular and orthopedic applications. The feasibility window for achieving the desired patterns with adequate geometrical fidelity was sought on the Mg alloys with difficult processability due to its low melting temperature and high thermal conductivity. Two different patterning strategies suited to scanner based processing were considered: i) a point by point strategy and ii) a continuous movement strategy. In order to demonstrate the high reproducibility along the scanned area, larger patches of 10 mm x 10 mm were textured using the developed methods.

2 Modelling and development of the DLIP system

2.1 DLIP based on Michelson-Morley interferometer

The new DLIP head is the combination of a Michelson-Morley interferometer with an industrial scanner head. In Figure 1 a schematic representation of the concept is reported. A collimated laser beam (d_c) at the output of beam expander is deflected to a beam splitter which is the first element of the Michelson-Morley interferometer dividing the incoming beam into two beams of half power. The two collimated beams of half power are reflected back to the beam splitter by two mirrors with a phase difference due to the optical delay between them. The optical path difference can be conveniently controlled by tilting one of the mirrors with respect to the vertical axis with an angle of (Figure 1). If θ is small, the half-power beams are combined on the far side of the beam splitter resulting in a collimated interfered beam, with a diameter of d_c and an interference angle of θ. In the combination zone interferences fringes appear with a periodicity in the millimetric scale.

The interference is realized between the two collimated beams, before the entrance of the scanner head. The handling of the collimated and interfered beams, through a scanner head, sets some constraints. Industrial scanner heads are generally characterized by an entrance hole sized in accordance with the dimensions of the galvanometric mirrors and f-theta lens that follow the optical path. The constrain given by the entrance hole of the scanner head is directly related to a restriction on the maximum interference angle, θ_{max}. The interference angle θ must be small enough to avoid vignette beams on the galvanometric mirrors. Based on this, the Michelson-Morley interferometer is adopted allowing small interference angles.

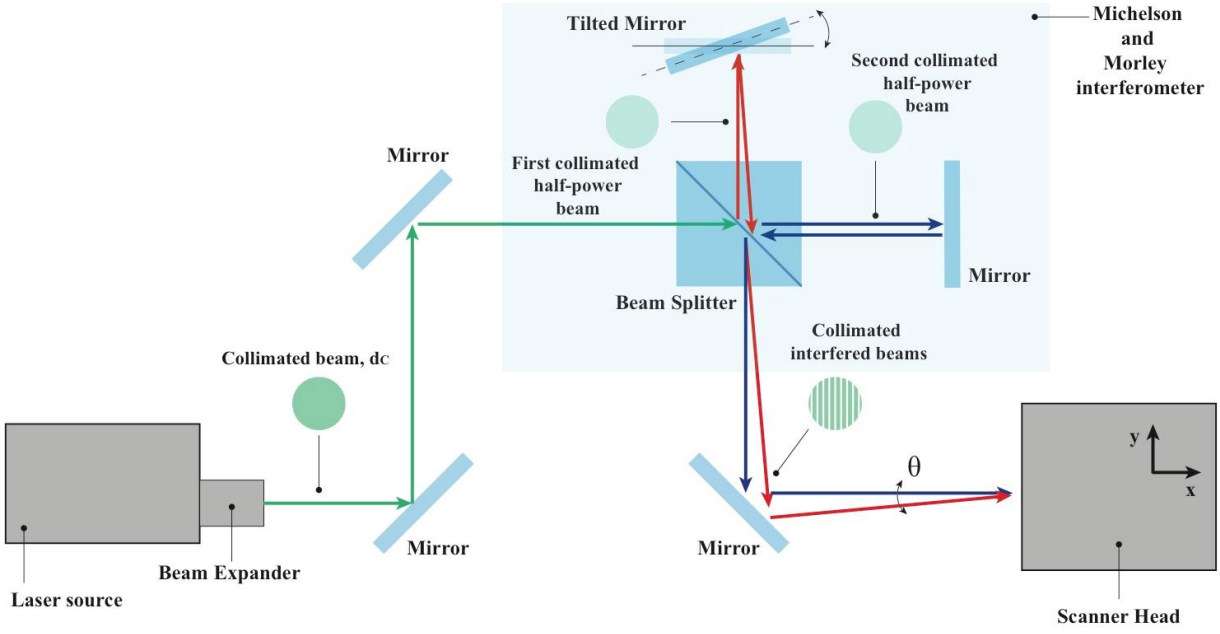

Figure 1 Schematic representation of employed DLIP system

If the sizing and the interference angles of the collimated beams are correctly done the interfering collimated beams can be launched into the scanner head and steered with conventional means employed for scanner heads. Once the interfering beams pass through the focusing f-theta lens the periodicity of the interference fringes are reduced due to the magnification factor of the lens. Hence a micrometric interfering beam is achieved on the workpiece with a micrometric to sub-micrometric periodicity of the interference pattern.

2.2 Design requirements and optical model of the new DLIP head

For the proposed DLIP concept the use of an f-theta telecentric lens is a constraint. When any laser beam hits the surface of an F-theta lens at an angle to the lens axis (Figure 2-a), this angle is traduced in a spot displacement at the flat target plane amplified by the focal length (f).

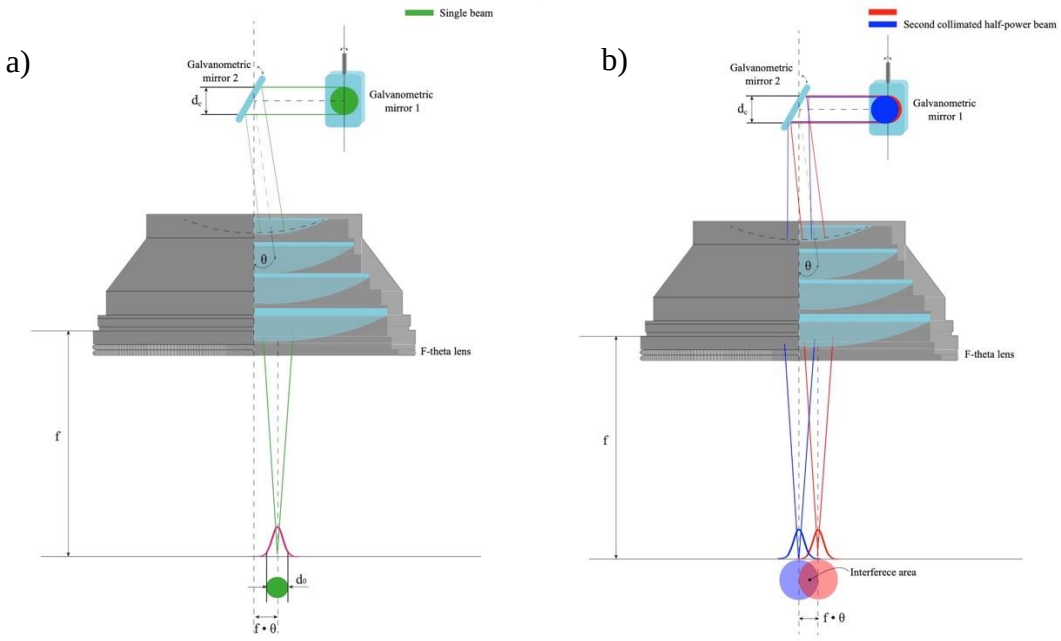

Figure 2 Schematic representation of an F-theta telecentric lens: a) with a single beam, b) with two interfered beams

This relation is the starting point of the optical model. In the present work the angle between the beams at the f-theta lens inlet is equal to the interference angle (θ). The spot displacement or the distance between the two interfering beams is (p) is:

$$p = f \cdot \theta \quad Eq.1$$

With two interfering beams at the focal point of the f-theta lens (Figure 2-b), beams may overall partially within their diameter. Nevertheless, beams interference requires the overlap of the beams. Consequently, the spot displacement (p) depends on the desired spot overlap (R) and the spot dimensions. Hence, at the target plane, the displacement p between the two focused beams is:

$$p = (1 - R) \cdot d_0 \quad Eq.2$$

where d_0 is the waist diameter obtained at the focal plane.

Starting from Eq.2, R=1 corresponds to complete spot overlapping, where consequently the interference angle is zero, hence, the phase difference cannot be regulated. For a controlled interference the conditions require that R<1 and p>0.
Putting together Eq.1 and Eq.2, the maximum value of interference angle θ_{max} can be calculated as a function of spot overlap (R) and focal length (f). If the laser source and the optical elements are fixed, waist diameter (d_0) and focal length (f) are constant, hence, the maximum interference angle only depends on the desired level of spot overlap (R):

$$\theta_{max} = (1 - R) \cdot \frac{d_0}{f} \quad Eq.3$$

that can be re-written as:

$$\theta_{max} = (1 - R) \cdot \frac{4\lambda M^2}{\pi d_c} \quad Eq.4$$

where M^2 is the beam quality factor and λ is the laser wavelength. Indeed, during the DLIP process the beam size can also be regulated by placing the workpiece away from the focal position. Hence, Eq.4 can be rewritten for a generic beam diameter on the workpiece d_w, for different focal positions (Δz [mm]). Starting from the caustic equation where:

$$d_w(\Delta z) = \sqrt{d_0^2 + \Delta z^2 \cdot \alpha^2} \quad Eq.5$$

where $\alpha \cong \frac{d_c}{f}$ is the divergence angle. At different focal positions, the maximum interference angle θ_{max} is expressed as:

$$\theta_{max} = (1 - R) \cdot \sqrt{\left(\frac{4\lambda M^2 f}{\pi d_c}\right)^2 + \Delta z^2 \cdot \left(\frac{d_c}{f}\right)^2} \cdot \frac{1}{f} \quad Eq.6$$

Having a maximum interference generates a limit to the minimum dimension of the pattern period. The minimum pattern period, Λ_{min}, can be calculated as:

$$\Lambda_{min} = \frac{\lambda}{2 \sin\left(\frac{\theta_{max}}{2}\right)} \cdot \frac{d_w}{d_c} \quad Eq.7$$

where $\frac{d_w}{d_c}$ is the magnification effect of F-theta lens, which is used as a scalability factor.
The Eq.7 can be read for a direct interpretation of the system specifications as it directly depends on laser characteristics and the optical component choices. Laser sources with a laser wavelength, λ, in the green or UV can help the process in the reduction of fringes size.
The beam quality factor M^2 also affects the model as an intrinsic property of the laser source. Industrial pulsed wave solid-state laser sources generally have a quasi-Gaussian energy distribution with an M^2 value close to 1.
If quasi-Gaussian beams realize interference, the energy redistribution is fringes modulated by the Gaussian profile. M^2 affects the process with an inhomogeneity between the central part of the beam spot and the annular one. On the other hand, decreasing R corresponds to a fringe period reduction. Nevertheless, lower overlap risks the process outcome as the interference should occur only in the tails of the Gaussian distribution.

Figure 3 shows the calculated pattern period as a function of laser wavelength, spots overlap, and focal position with fixed levels of M^2=1.2, d_c=10 mm and f=100 mm operating at θ_{max}. For instance fixing conveniently the focal position on 2 mm and the overlap on 0.77, the pattern period is 46.5 μm with $\lambda = 1064\ nm$. With shorter wavelength such as 532 nm and 355 nm, pattern period reduces respectively to 23 μm and 15 μm. Moreover, reducing R to 0.5 further decreases pattern periods. Fixing laser wavelength on 532 nm and R on 0.5 the pattern period becomes 10.6 μm.

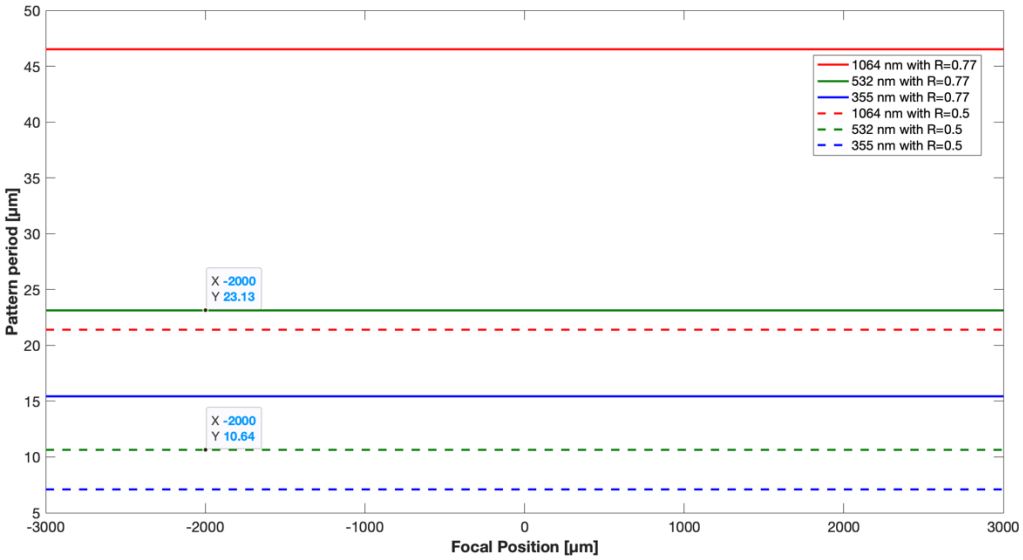

Figure 3 Pattern period for different laser wavelength and overlap considering interference at θ_{max} (M^2=1.2, d_c=10 mm, f=100 mm)

The dimension of collimated beams, as much as the focal length of the f-theta lens, affects patterns size. Increasing d_c decreases fringes period, while increasing f increases fringes period. Figure 4 shows the relationship between pattern period and d_c and f. The trends are plotted considering $\lambda = 532\ nm$, M^2=1.2, and R=0.77, operating at θ_{max}. Figure 4-a shows an enlarged pattern period decreasing d_c. The pattern period passes from 23 µm to 46 µm when dc moves from 10 mm to 5 mm. Figure 4-b shows a reduced pattern period decreasing f. The pattern period passes from 23 µm to 12 µm when f moves from 100 mm to 50 mm. Accordingly it can be seen that larger collimated beams and shorter focal lengths are favorable also for reducing the pattern period.

a)

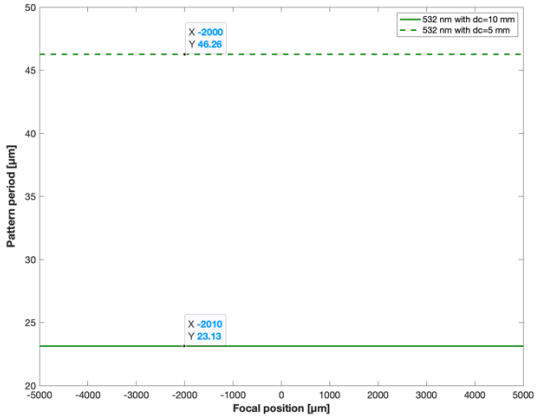

b)

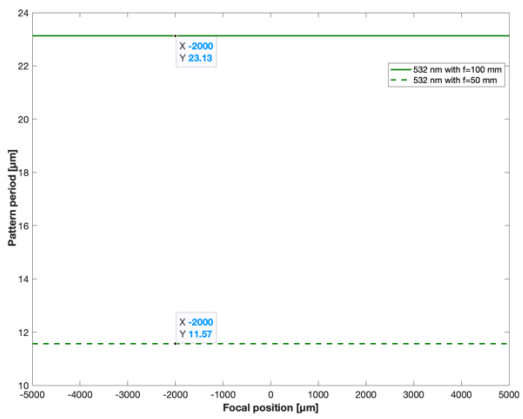

Figure 4 Pattern period as a function of: a) dc, b) f ($\lambda = 532\ nm$, M^2=1.2, R=0.77, operating at θ_{max})

2.3 Implemented DLIP system

The designed and integrated DLIP system was based on a compromise between the different design requirements. A Q-switched ns-pulsed diode pumped solid state Nd:YVO_4 green laser was found to be suitable both for the pattern period, power levels achievable, and due to the compactness of the overall solution in view of industrial applications (Innolas – Nanioair 532-10-V). The laser emits the green light at 532 nm as laser wavelength. The 30 ns pulses are long enough to maintain spatial pulse overlap without excessive difficulty in the alignment. In fact, in DLIP, the parameters of the pulsed laser source are crucial (i.e. pulse repetition rate PRR, and pulse duration τ). In DLIP to guarantee beam interference, it is necessary to have partial or complete temporal overlap. The overlapped area is directly connected to the optical path difference of two interference beams and the difference can correspond to a temporal delay and, consequently, to an absence of overlap between the two beams. The maximum optical path difference was determined by $\Delta x_{max} = c \cdot \tau$, where c is the speed of light. Considering a $\tau = 30\ ns$ and the desired temporal overlap at 99% the maximum optical path difference is $\Delta x_{max} \cong 90\ mm$. In the present combination, the wavelength and the pulse duration provides a moderate micromachining quality compared to ns-pulsed NIR fiber laser sources and ease of operation compared to ps or fs pulsed ultrafast lasers.

Table 1 details the features of the employed laser source. A beam expander with 10X magnification increases the diameter of the collimated laser beam before entering the Michelson-Morley interferometer. The recombined spot passes throughout the entrance hole of the 2-axis scanner head (Cambridge Technology- ProSeries1). An F-theta telecentric lens with a focal length of 100 mm focuses the beam spot. Figure 1 shows the schematic representation of employed set-up. In the current configuration the maximum angle and the minimum period were 0.026° and 23.1 μm, considering R=77%. In the present work, all energy levels are referred to the measurements taken after the beam expander.

Parameter	**Symbol**	**Value**
Wavelength	λ	532 nm
Pulse duration	τ	<30 ns
Pulse repetition rate	PRR	20-200 kHz
Beam quality factor	M^2	1.2
Maximum average power	P_{avg}	10 W
Collimated diameter	d_c	10 mm
Polarization		Linear
Maximum interference angle	θ_{max}	0.026°
Minimum pattern periodicity at R=77%	Λ_{min}	23.1 μm

Table 1 Characteristics of the employed diode pumped solid state Nd:YAG laser source

The employed laser was controllable through the pump current (PI%) of the pumping diodes and pulse repetition rate (PRR) of the acousto-optic Q-switching system. In combination the laser energy was varied. However, the laser emitted the first pulse with an overshoot of higher an energy compared to the rest of the pulses in the train. Such overshooting or ramped profiles can be associated to the functioning principle of the pumping system or the amplifier media [40], [41]. The energy of the first pulse depended on the combination of PI% and PRR. In Figure 5 the characteristic emission profile of the employed pulsed laser source is shown. It can be seen that after the initial overshooting pulse the following pulses are emitted with a stable variability within the pulse train.

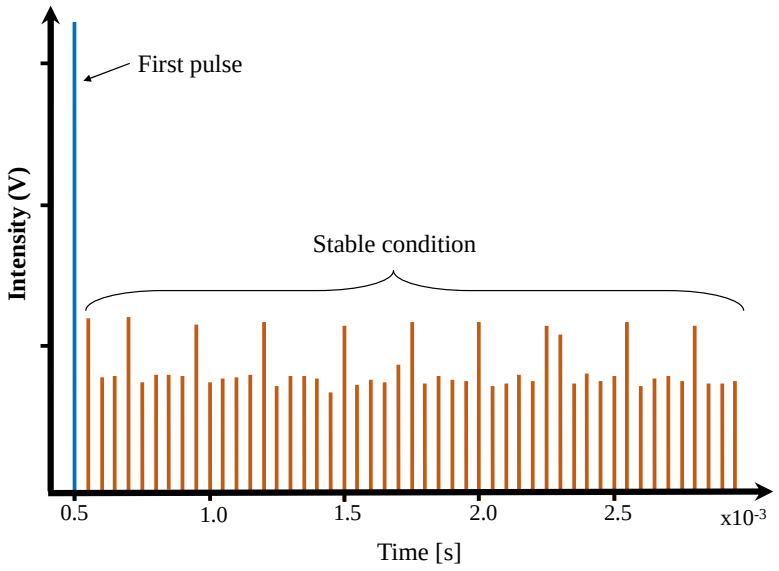

Figure 5 The characteristic emission profile of the employed green laser source observed by a fast photodiode (PI%=80, PRR=20 kHz)

The emission profile of the laser source was characterized and regulated for the experimental work at PRR=20 kHz. Figure 6 shows the energy content of the first pulse compared with stable pulses as a function of PI%. The first pulse was characterized by a higher amount of energy for PI% between 60%-90%. Between 95% and 100% of PI% the overshooting first peak was not observed. This profile was exploited to test higher energies concerning single pulsed emission profiles.

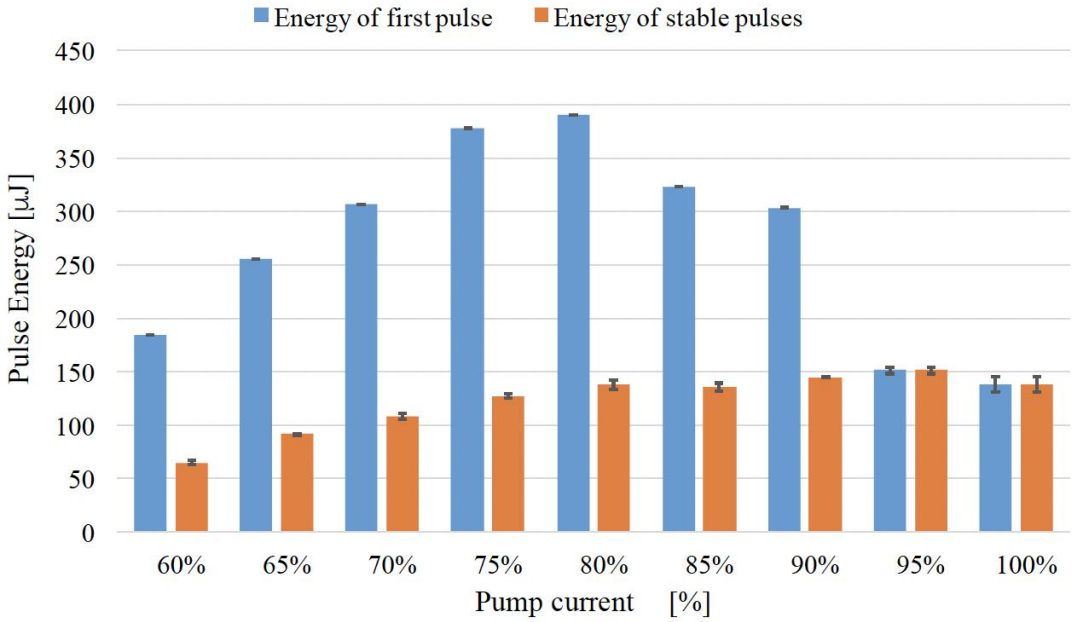

Figure 6 First pulse energy compared with stable pulses energy, as a function PI% for a fixed PRR=20 kHz

3 Materials and Methods

3.1 Materials

The employed material was the biodegradable magnesium alloy AZ31 (Al 3 wt%, Zn 1 wt%, Mg bal). DLIP process patterns cold-rolled sheets with 0.2 mm thickness. The AZ31 presents some critical aspects: low melting temperature (T_m=905 K) and high thermal conductivity (k=96 W/mK).

Previous works investigated these aspects in the DLIP process [36],[37]. The production of micro, sub-micro, and nanometric surface patterns are highly exploitable for regulating the biological performance and biodegradation behavior of the material.

3.2 Experimental procedure

When ns-pulsed lasers are employed, the thermal ablation process may generate dross and recast in conventional micromachining operations. In DLIP such defects may result in the filling of the interference patterns resulting in reduced process resolution. Such issues are amplified when the AZ31 Mg alloy is considered due to its low melting temperature and high heat conductivity making it prone to excessive melt generation. In two-beam DLIP the intensity of the interference beams in the constructive areas is theoretically two times the interference of the original beam [42]. The increment of the intensity profile combined with the material results in a strong influence of the parameters on melting phenomena and pattern quality. During the ablation-based process, the modified fluence profile of the beam overcomes the ablation threshold locally resulting in material removal with a patterned profile [42]. Hence, the pattern width and periodicity are smaller than the size of the beam. For the same interaction mechanism, the size of the interacted region can be smaller than the size of the beam. With ns-long pulses the material removal mechanism is more complex than a direct ablation and it is based on vaporization and melt expulsion. Hence, the observed pattern is expected to be a combination of material removed by vaporization and melt expulsion and material remodeled by the melt flow. Hence a careful study concerning the energy intensity deployed to during the DLIP process is required. For this purpose the laser energy and beam size should be adjusted.

For a greater control of the laser energy in space two scanning strategy were investigated namely "point by point" and "continuous scanning".

Point by point strategy investigates the influence of one or two pulses considering the behavior of the emission profile described in the previous section where the energy content of the first pulse is exploited (Figure 6). Moreover, *Point by point* (Figure 7-a) is a method, generally used in precise percussion drilling operations or in laser surface texturing concerning dimple geometries [40]. The laser beam moves to a position, laser exposure is applied with a fixed energy (E) and number of pulses (N), and later the beam jumps to a consecutive position along the scan direction or to the next hatch line. To achieve a complete surface patterning operation, the spots need to overlap both along the scanning (x) and the hatch (y) directions.

The second approach exploits a continuous movement of the galvo mirrors during the emission of the laser (Figure 7-b), which is the common laser scanning approach used for engraving and marking operations. In *continuous scanning*, the beam is moved on the scan direction from the beginning to the end of the hatch line. Once the hatch line is completely scanned, the laser jumps to the consecutive hatch line. In this approach, the pulse energy is related to the stable part of the train (Figure 6).

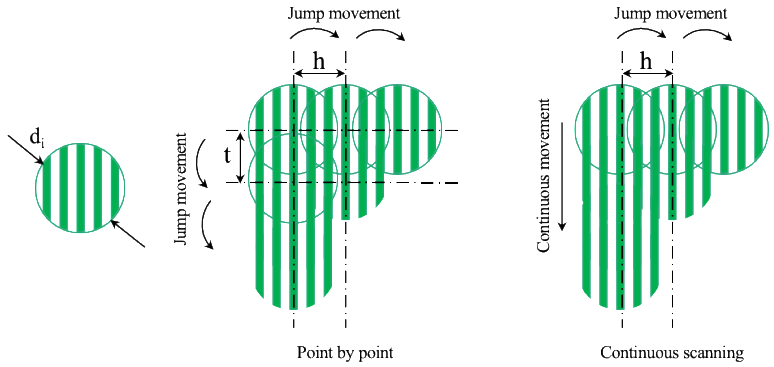

Figure 7 Schematic representation of adopted scanning strategies: "point by point" and "continuous scanning"

In order to assess the feasibility window of the "point by point" strategy, laser pulse energy (E), number of pulses (N), and focal position (Δz) were varied. In order to apply 2 pulses, a delay time was employed between the consecutive pulses to exploit the same high energy content of the first pulse of the train. Fixed parameters are the interference angle (θ) and the pulse repetition rate (PRR), respectively 0.026° and 20 kHz. Table 2 reports the experimental conditions of the feasibility window for the "point by point" approach.

Fixed parameters		
Pulse Repetition Rate	PRR	20 kHz
Interference angle	θ	0.026°
Varied parameters		
Pulse energy	E	138 μJ – 390 μJ
Number of pulses	N	1, 2
Focal position	Δz	1.0, 1.5, 2.0, 2.5, 3 mm

Table 2 Experimental conditions of "point by point" DLIP feasibility window characterization

For the *continuous scanning*, the feasibility window was sought by varying the laser energy (E), focal position (Δz), and marking speed (v). The effect of the first pulse of the emission profile was negligible concerning the total interaction time along the beam path. Fixed parameters were the interference angle (θ) and the pulse repetition rate (PRR), respectively 0.026° and 20 kHz. Table 3 reports the experimental conditions of the feasibility window.

Fixed parameters		
Pulse Repetition Rate	PRR	20 kHz
Interference angle	θ	0.026°
Varied parameters		
Pulse energy	E_{st}	65 μJ – 151μJ,
Marking speed	v	10 mm/s – 500 mm/s
Focal position	Δz	1.5, 2.0, 2.5, 3 mm

Table 3 Experimental conditions of "continuous scanning" DLIP feasibility window characterization

All patterns were acquired via SEM (EVO-50 from Carl Zeiss, Oberkochen, Germany) The quality of the periodic structures were classified for both of the strategies. Machining rates were calculated for the two selected conditions as described by Maressa et al [43].
After the determination of the feasibility window, larger areas were patterned (10 mm x 10 mm) for analyzing pattern consistency. The interference angle was 0.026°. The overlap between the interfering beams was $d_i = 0.77 \cdot d_w$ where d_w was 200 μm at a focal distance of 2 mm. In this configuration, the pattern periodicity was 23.1 μm. The overlap between two consecutive points in point by point strategy namely the pitch distance was equal to 75 μm. The distance between the consecutive tracks in both of the strategies namely the hatch distance was 75 μm. In point by point strategy the value of jump delay was set to 100 μs to ensure the emission of the high energy pulse [44]. Table 4 report the selected condition for each strategy.
SEM images of the produced patterns were taken. Pattern periodicity was measured using these images with image processing software. Five tracks were measured in three different regions to calculate the average value.

Parameter	**Symbol**	**Point by point**	**Continuous scanning**
Overlap	R%	77%	77%

Interference angle	θ	0.026°	0.026°
Number of pulse	N	1	n/a
Pulse repetition rate	PRR	20 kHz	20 kHz
Stable energy	E_{st}	108 μJ	92 μJ
Focal position	Δz	2 mm	2 mm
Beams spot	d_w	200 μm	200 μm
Interference spot	d_i	154 μm	154 μm
Jump delay	J_d	100 μs	n/a
Mark speed	v	n/a	150 mm/s
Hatch distance	h	75 μm	75 μm
Pitch	t	75 μm	n/a
Theoretical pattern period	Λ	23.1 μm	23.1 μm

Table 4 Selected conditions for larger area patterning.

4 Results and discussion

4.1 Two-beam DLIP feasibility window for "point by point" strategy

The obtained surfaces were classified qualitatively as a function of pattern quality. Four categories are defined as follows:

- Incomplete patterns: This is the case of surfaces with discontinuous patterns. This condition occurs when the energy content is not enough to produce the desired interaction between the interference beams and the material. In the incomplete patterns, the areas of constructive interference partially interact with the target material with uncomplete treatments of the magnesium alloy. Particularly the discontinuities are more present on the annulus of the interference spot, due to the reduced content of energy in the irradiance profile.
- Line-like patterns: This is the case of surfaces with well-defined line-like periodic patterns. The areas of constructive and destructive interference are detectable and measurable. In this condition the interference beams interact properly with the material; the areas of constructive interference remove the magnesium with melting and vaporization phenomena, while the areas of destructive interference do not interact with the target material. It is the desired class.
- Melted patterns: Melted patterns are characterized by line-like patterns where the areas of destructive interference are fully or partially filled by molten material. This condition is undesirable due to its low precision.
- Un-patterned: this is the case where the interference beams are not able to produce any periodic structures on the target surface. This condition occurs in two different cases: i) lower energy content, ii) higher energy content. Low energy content does not permit the interaction between the interference beams and material resulting in untreated surfaces. High energy content produces strong interaction between the interference beams and the material resulting in uncontrolled material ablation. This class is not acceptable.

Figure 8 shows the representative pictures of classified conditions. The classification of surfaces identifies the feasibility map of point by point DLIP process. The increase of pulse energy shows a transition from line-like patterns to melted patterns to un-patterned. The energetic content increases for focal positions that are lower than 2 mm. Melted patterns and un-patterned are present for different energetic levels. Moreover, few cases of incomplete patterns are present. The interaction between a ns pulsed laser source and a metallic material, like magnesium involves the presence of

molten material and its flux. Particularly, the Marangoni convection is a driving mechanism [45]. Marangoni convection describes the flow of molten material from the region with constructive interference, to the region with destructive interference. This material redistribution became more relevant with the energy content. This is more visible in un-patterned and melted patterns. In the focal positions closed to the waist diameter ($\Delta z \leq 1$ mm), beams are partially overlapped according to the optical model as seen in Figure 9. With an increase of number of pulses at N=2, a narrow set of parameters produces line-like patterns. The un-patterned condition is observed more frequently. Apparently the second pulse seems to degrade the initially line-like patterns, which may also be related to the energy fluctuations between the initial few pulses of the laser sources. With N=2 line-like patterns are limited to a few levels of focal position and the lower condition of pulse energy.

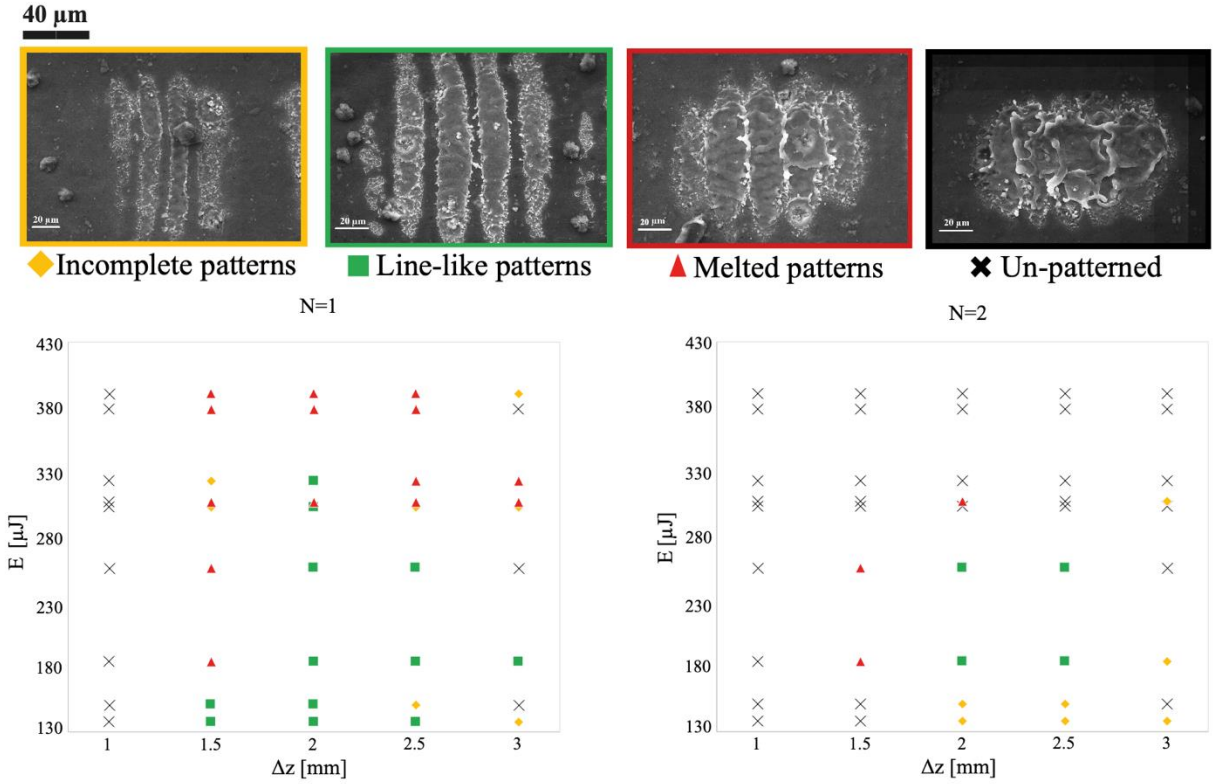

Figure 8 Feasibility map of "point by point" DLIP process. On the top: the four categories for pattern quality classification, on the bottom: the two feasibility windows as a function of varied parameters

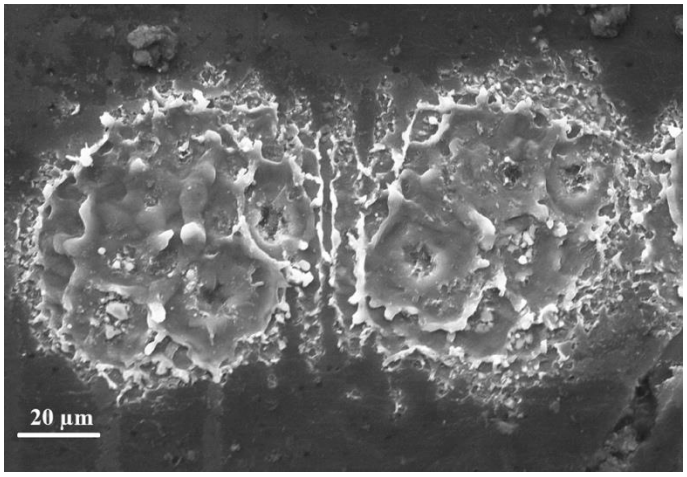

Figure 9 Partial overlap of interfered spots for Δz=1 mm

4.2 Two-beam DLIP feasibility window for "continuous scanning" strategy

A similar qualitative classification was carried out also for the "continuous scanning" strategy as described in the following.

- Incomplete patterns: this class is the defined as the same way as in "point by point strategy". It is an undesired condition.
- Line-like patterns: this class is the defined as the same way as in "point by point strategy".
- Melted patterns: this class is the defined as the same way as in "point by point strategy". It is an undesired condition.
- Ablated patterns: this class occurs with a strong energy content generating excessively melted material and deep grooves. It is an undesired condition.
- Un-patterned: this class is the defined as the same way as in "point by point strategy". It is an undesired condition.

Figure 10 shows representative images of the classified conditions along with the feasibility map of the *continuous scanning* strategy.

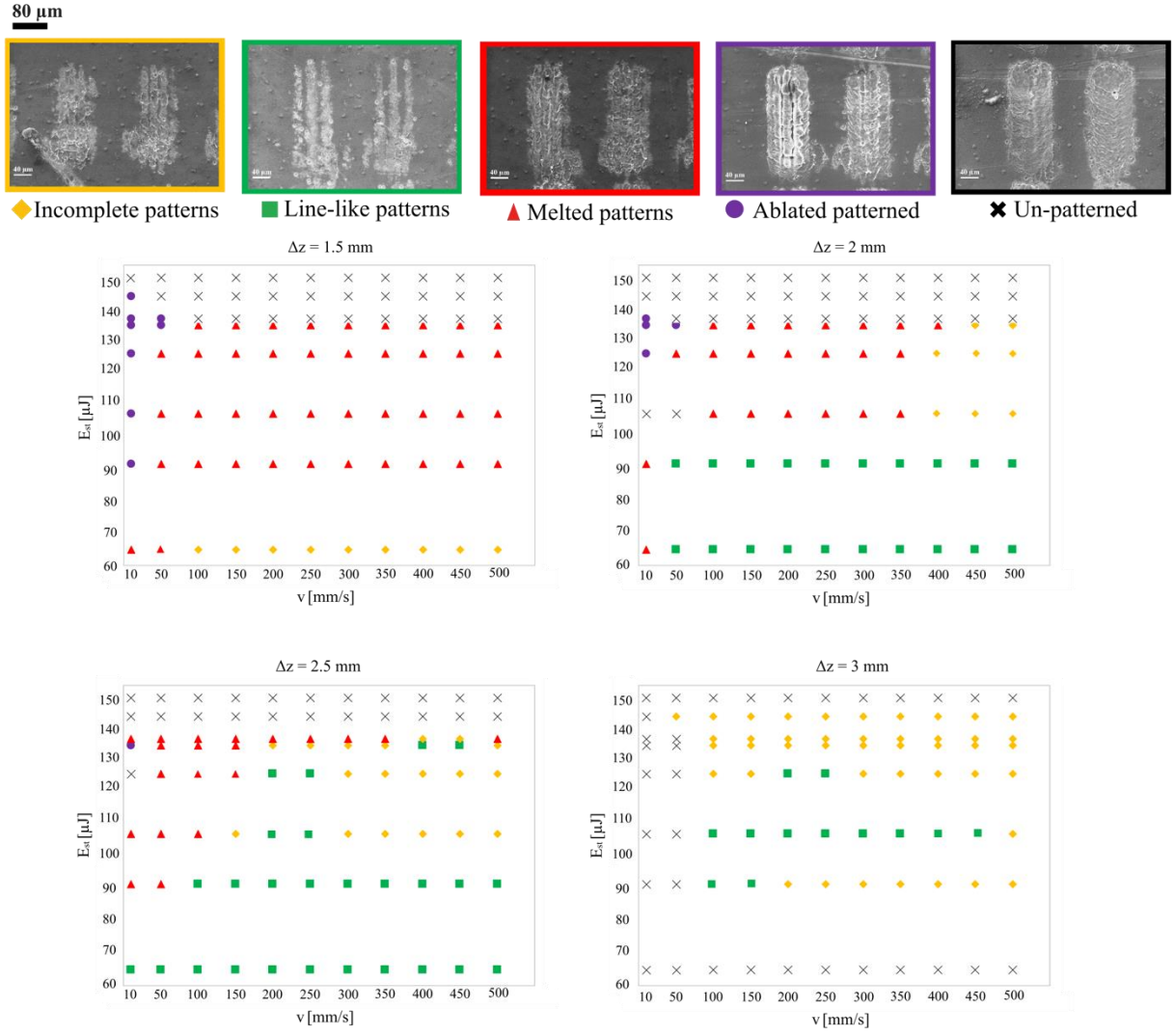

Figure 10 Feasibility map of "continuous scanning" DLIP process. On the top: the four categories for pattern quality classification, on the bottom: the two feasibility windows as a function of varied parameters

It can be seen that the focal position strongly affected the processability. Lower values of Δz correspond to higher beam intensities where surfaces melted or deeply ablated. On the other hand, the highest Δz values reduces the beam intensity to a degree, where line-like patterns are not present, moving directly to incomplete patterns or absent treatments. Accordingly, the efficacies of the pulse

energy and scan speed become relevant when the Δz values in the convenient region (2-2.5 mm) and the work diameter is sufficiently large. In this range, the process can be scaled up to 500 mm/s, providing highly promising results for improved productivity.

4.3 Patterning quality with scanning optics

Figure 11 shows the samples manufactured over 10 mm x 10 mm area with the two strategies. Both of the surfaces appear to be homogenous with a difference in the morphology of the machining process throughout the surface. The surfaces show a larger fraction of melted material compared to the feasibility window experiments. This is attributed to the use of multiple tracks and overlapping regions between the tracks resulting in a more consistent molten material flow. The periodicity measurements showed a $\Lambda_{\text{point by point}} = 22.6\ \mu\text{m} \pm 0.14\ \mu\text{m}$ and $\Lambda_{continuous} = 22.8\ \mu m \pm 1.03\ \mu m$. Both conditions appear adequately close to the theoretical value of the interference pattern. Nevertheless, the continuous scanning strategy appears to provide smaller quantity of melted material flowing back to the previously machine interference patterns, hence a relatively better quality. In the continuous scanning strategy, the areas of constructive and destructive interference are more homogeneous in both directions. The point by point strategy requires the alignment of the interference pattern between each exposure points. Each jump of the laser beam between consecutive exposure points requires a correct position, which may lower the overall precision of the pattern. Figure 12 reports the periodicity and machining rate comparisons It can be seen that the continuous scanning strategy provides adequate quality at much higher machining rate as it avoids idle times between exposure points. The DLIP strategy with scanning optics adequately fits the purpose with a scan strategy close to what is employed in laser marking and engraving processes. This implies that the processing of large areas with designed surface geometries can be readily processed with DLIP employing conventional scanning methods based on vector based hatching.

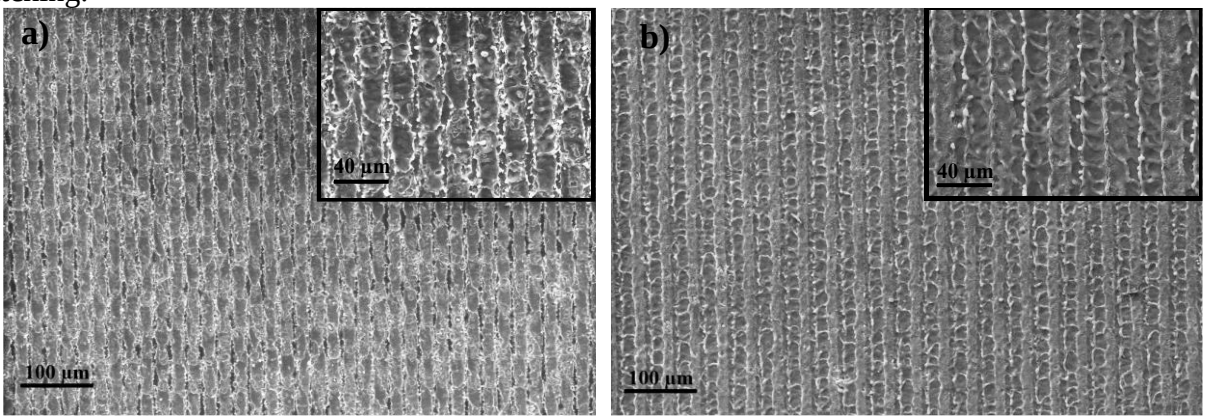

Figure 11 Large area fabrication with a) "Point by point" strategy, and b) "Continuous scanning" strategy

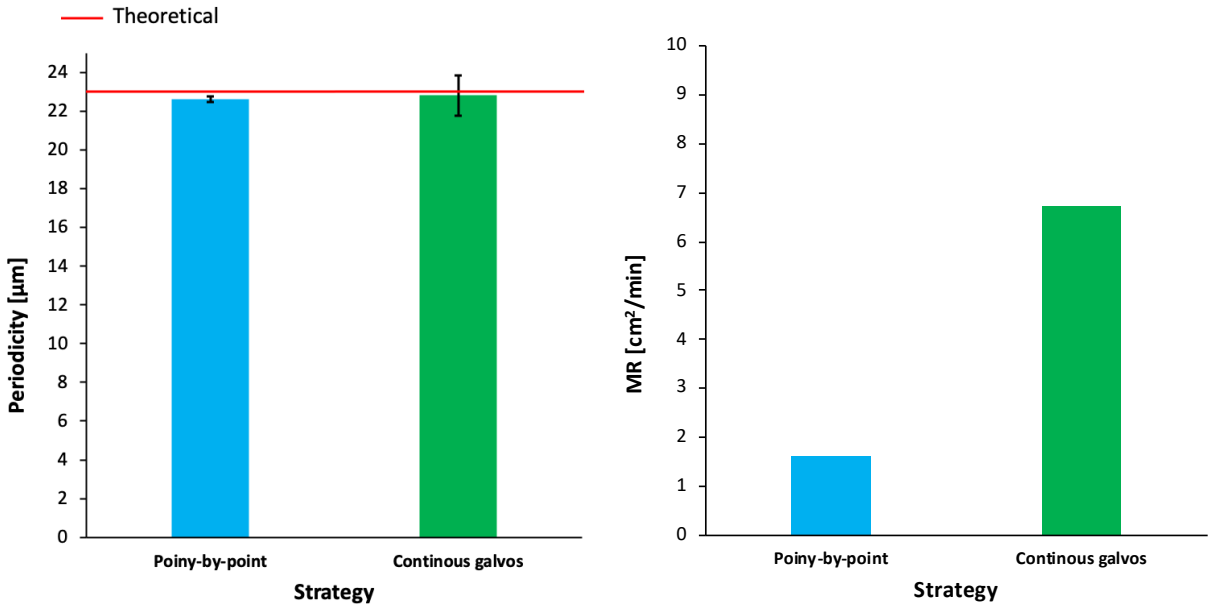

Figure 12 Comparison of periodicity and machining rate (MR) for the two employed strategies.

The obtained periodicity on magnesium alloy is ~23 μm, relatively large compared to the DLIP applications shown in the literature. This is a consequence of the limited angular difference between the two beams in the Michelson-Morley interferometer. While, the current work shows the proof-of-concept with a large periodicity, it indicates the ways for further period reduction by means of optical design changes. On the other hand, the obtained pattern period can be readily employed in in the field of biodegradable implants. An example can be the adhesion and proliferation of endothelial cells, where linear patterns with a periodicity similar to the cell size has been shown to be advantageous [46]. Similarly, such patterns can be exploited for improving the adhesion of polymeric coatings on the Mg-alloys to regulate the biodegradation rate [4].

5 Conclusions

In this work, a novel DLIP approach based on Michelson-Morley interferometer and scanning optics has been systematically developed from modelling to the processing. The following points summarize the main outcomes of the work.

- The Michelson-Morley interferometer can be exploited to generate the angular difference between two interfering beams prior to launching into a scanner head. The scanner head than allows to reduce the pattern period and machine large areas.
- In the proposed DLIP system, beam wavelength and quality are considered design parameters effecting the maximum interference angle allowed by the scanner beam input.
- A green laser beam with a conventional focal length at 100 mm provide micrometric pattern periodicity suitable for parallel machining of multiple lines. In order to move towards smaller periods shorter focal lenses and wavelengths can be preferred.
- The feasibility on the employed Mg alloy depended majorly on the beam intensity regulated by the focal distance. Both the point by point and continuous scanning strategies were able to generate the periodic patterns in their own feasibility windows.
- The larger area fabrication showed that with adequate choice of the process parameters, it is potentially possible to homogenously machine large areas, while the scan strategy determines the productivity mainly.
- The continuous scanning strategy proved that DLIP can be flexibly operated using conventional scanner and control software with vector hatching strategies.

While the present work shows the overall feasibility, the presented DLIP approach requires further attention towards sub-micrometric and nanometric resolution. The use of larger scanner apertures,

shorter wavelengths, and focal distances can provide the means to further periodicity reduction. The combination of a larger number of beams can also be foreseen, while it is expected to further complicate the optical design.

Acknowledgements

The authors would like to acknowledge Innolas and Optoprim Srl for the collaboration and the support provided.

References

[1] Y. Wan and D. S. Xiong, "The effect of laser surface texturing on frictional performance of face seal," *J. Mater. Process. Technol.*, vol. 197, pp. 96–100, 2008.

[2] F. A. Lasagni and A. F. Lasagni, *Fabrication and Characterization in the Micro-Nano Range*, vol. 5. 2010.

[3] A. G. Demir, P. Maressa, and B. Previtali, "Fibre laser texturing for surface functionalization," in *Physics Procedia*, 2013, vol. 41, pp. 759–768.

[4] A. G. Demir *et al.*, "Laser surface structuring affects polymer deposition, coating homogeneity, and degradation rate of Mg alloys," *Mater. Lett.*, vol. 160, pp. 359–362, 2015.

[5] T. Yong Hwang *et al.*, "Enhanced efficiency of solar-driven thermoelectric generator with femtosecond laser- textured metals," *J. Phys. Chem. B Sol. Cells Sci. Sol. Energy Mater. Adv. Mater. (deerf. Beach Fla.) A. Reja R. J. Ram*, vol. 114, no. 7, pp. 14339–14342, 2010.

[6] L. Yalçin and R. Öztürk, "Performance comparison of c-Si, mc-Si and a-Si thin film PV by PVsyst simulation," *J. Optoelectron. Adv. Mater.*, vol. 15, no. 3–4, pp. 326–334, 2013.

[7] L. Luo, Z. Jiang, D. Wei, and X. He, "Surface modification of titanium and its alloys for biomedical application," *Adv. Mater. Reserach*, vol. 888, pp. 1115–1120, 2014.

[8] C. De Giorgi, V. Furlan, A. G. Demir, E. Tallarita, G. Candiani, and B. Previtali, "Laser Micro-polishing of Stainless Steel for Antibacterial Surface Applications," *Procedia CIRP*, vol. 49, pp. 88–93, 2016.

[9] S. Okazaki, "High resolution optical lithography or high throughput electron beam lithography: The technical struggle from the micro to the nano-fabrication evolution," *Microelectron. Eng.*, vol. 133, pp. 23–35, 2015.

[10] T. Li, M. Paliy, X. Wang, B. Kobe, W. M. Lau, and J. Yang, "Facile One-Step Photolithographic Method for Engineering Hierarchically Nano/Microstructured Transparent Superamphiphobic Surfaces," *ACS Appl. Mater. Interfaces*, vol. 7, no. 20, pp. 10988–10992, May 2015.

[11] M. S. Kim *et al.*, "Preparation of fluoropolymer structures for orthogonal processing of diverse material by Micro-Contact Printing," *Microelectron. Eng.*, vol. 123, pp. 33–37, 2014.

[12] Y. Li, H. W. Ng, B. D. Gates, and C. Menon, "Material versatility using replica molding for large-scale fabrication of high aspect-ratio, high density arrays of nano-pillars," *Nanotechnology*, vol. 25, no. 28, 2014.

[13] C. Marzolin, S. P. Smith, M. Prentiss, and G. M. Whitesides, "Fabrication of glass microstructures by micro-molding of sol-gel precursors," *Adv. Mater.*, vol. 10, no. 8, pp.

571–574, 1998.

[14] M. Röhrig *et al.*, “Hot pulling and embossing of hierarchical nano- and micro-structures,” *J. Micromechanics Microengineering*, vol. 23, no. 10, pp. 105014–105021, Oct. 2013.

[15] R. Bruck and R. Hainberger, “Direct replication of nanostructures from silicon wafers in polymethylpentene by injection molding,” *SPIE Opt. ...*, vol. 43, no. Cd, 2010.

[16] B. Wu, M. Zhou, J. Li, X. Ye, G. Li, and L. Cai, “Superhydrophobic surfaces fabricated by microstructuring of stainless steel using a femtosecond laser,” *Appl. Surf. Sci.*, vol. 256, pp. 61–66, 2009.

[17] K. Ahmmed, C. Grambow, and A.-M. Kietzig, “Fabrication of Micro/Nano Structures on Metals by Femtosecond Laser Micromachining,” *Micromachines*, vol. 5, no. 4, pp. 1219–1253, Nov. 2014.

[18] M. Mastellone *et al.*, “Deep-Subwavelength 2D Periodic Surface Nanostructures on Diamond by Double-Pulse Femtosecond Laser Irradiation,” *Nano Lett.*, vol. 21, pp. 4477–4483, 2021.

[19] Q. Liu, X. Duan, and C. Peng, *Novel Optical Technologies for Nanofabrication*. 2014.

[20] B. Voisiat, W. Wang, M. Holzhey, and A. F. Lasagni, “Improving the homogeneity of diffraction based colours by fabricating periodic patterns with gradient spatial period using Direct Laser Interference Patterning,” *Sci. Rep.*, vol. 9, no. 7801, pp. 2–10, 2019.

[21] D. W. Müller, T. Fox, P. G. Grützmacher, S. Suarez, and F. Mücklich, “Applying Ultrashort Pulsed Direct Laser Interference Patterning for Functional Surfaces,” *Sci. Rep.*, vol. 10, no. 1, pp. 1–14, 2020.

[22] M. R. S. Castro, A. F. Lasagni, H. K. Schmidt, and F. Mücklich, “Direct laser interference patterning of multi-walled carbon nanotube-based transparent conductive coatings,” *Appl. Surf. Sci.*, vol. 254, no. 18, pp. 5874–5878, 2008.

[23] A. F. Lasagni, J. L. Hendricks, C. M. Shaw, D. Yuan, D. C. Martin, and S. Das, “Direct laser interference patterning of poly(3,4-ethylene dioxythiophene)-poly(styrene sulfonate) (PEDOT-PSS) thin films,” *Appl. Surf. Sci.*, vol. 255, no. 22, pp. 9186–9192, 2009.

[24] S. Eckhardt, C. Sachse, and A. F. Lasagni, “Light management in transparent conducting oxides by direct fabrication of periodic surface arrays,” *Phys. Procedia*, vol. 41, pp. 552–557, 2013.

[25] M. D’Alessandria, A. Lasagni, and F. Mücklich, “Direct micro-patterning of aluminum substrates via laser interference metallurgy,” *Elsevier*, 2008.

[26] A. Lasagni, M. Cornejo, F. Lasagni, and F. Muecklich, “Laser Ablation Modeling of Periodic Pattern Formation on Polymer Substrates,” *Adv. Eng. Mater.*, vol. 10, no. 5, pp. 488–493, 2008.

[27] M. Bieda, E. Beyer, and A. F. Lasagni, “Direct Fabrication of Hierarchical Microstructures on Metals by Means of Direct Laser Interference Patterning,” *J. Eng. Mater. Technol.*, vol. 132, no. 3, pp. 031015–6, 2010.

[28] C. Gachot, R. Catrin, A. Lasagni, U. Schmid, and F. Mücklich, “Comparative study of grain sizes and orientation in microstructured Au, Pt and W thin films designed by laser interference metallurgy,” *Appl. Surf. Sci.*, vol. 255, no. 10, pp. 5626–5632, 2009.

[29] L. Muller-Meskamp *et al.*, “Transparent Conductive Metal Thin-Film Electrodes Structured by Direct Laser Interference Patterning **,” *Wiley Online Libr.*, vol. 17, no. 8, pp. 1215–1219, Aug. 2015.

[30] L. Müller-Meskamp *et al.*, “Efficiency enhancement of organic solar cells by fabricating

periodic surface textures using direct laser interference patterning," *Adv. Mater.*, vol. 24, no. 7, pp. 906–910, 2012.

[31] M. Duarte, A. Lasagni, R. Giovanelli, J. Narciso, E. Louis, and F. Mücklich, "Increasing Lubricant Film Lifetime by Grooving Periodical Patterns Using Laser Interference Metallurgy**," *Wiley Online Libr.*, vol. 10, no. 6, pp. 554–558, Jun. 2008.

[32] M. Bieda, C. Schmädicke, T. Roch, and A. Lasagni, "Ultra-low friction on 100Cr6-steel surfaces after direct laser interference patterning," *Adv. Eng. Mater.*, vol. 17, no. 1, pp. 102–108, Jan. 2015.

[33] E. A. Bremus-Koebberling, S. Beckemper, B. Koch, and A. Gillner, "Nano structures via laser interference patterning for guided cell growth of neuronal cells," *J. Laser Appl.*, vol. 24, no. 4, p. 042013, Sep. 2012.

[34] A. Lasagni *et al.*, "Bringing the Direct Laser Interference Patterning Method to Industry: a One Tool-Complete Solution for Surface Functionalization," *JLMN-Journal of Laser Micro/Nanoengineering*, vol. 10, no. 3, 2015.

[35] A. Lasagni, T. Roch, J. Berger, and T. Kunze, "To use or not to use (direct laser interference patterning), that is the question," *spiedigitallibrary.org*, 2015.

[36] V. Lang, T. Roch, and A. F. Lasagni, "World record in high speed laser surface microstructuring of polymer and steel using direct laser interference patterning," vol. 9736, no. 0, p. 97360Z, 2016.

[37] A. F. Lasagni *et al.*, "Large area micro-/nano-structuring using direct laser interference patterning," vol. 9735, no. 0, p. 973515, 2016.

[38] T. Kunze, C. Zwahr, B. Krupop, S. Alamri, F. Rößler, and A. F. Lasagni, "Development of a scanner-based direct laser interference patterning optical head: new surface structuring opportunities," p. 1009214, 2017.

[39] S. Alamri, A. I. Aguilar-morales, and F. Rößler, "Biomimetic Surface Structuring Using Laser Based Interferometric Methods," *Appl. Sci.*, vol. 8, no. 1260, pp. 1–14, 2018.

[40] A. G. Demir, B. Previtali, and N. Lecis, "Development of laser dimpling strategies on TiN coatings for tribological applications with a highly energetic Q-switched fibre laser," *Opt. Laser Technol.*, vol. 54, pp. 53–61, 2013.

[41] A. G. Demir, K. Pangovski, W. O'Neill, and B. Previtali, "Laser micromachining of TiN coatings with variable pulse durations and shapes in ns regime," *Surf. Coatings Technol.*, vol. 258, pp. 240–248, 2014.

[42] V. Furlan, M. Biondi, A. G. Demir, G. Pariani, B. Previtali, and A. Bianco, "Sub-micrometric surface texturing of AZ31 Mg-alloy through two-beam direct laser interference patterning with a ns-pulsed green fiber laser," *Appl. Surf. Sci.*, vol. 423, 2017.

[43] P. Maressa, L. Anodio, A. Bernasconi, A. G. Demir, and B. Previtali, "Effect of surface texture on the adhesion performance of laser treated Ti6Al4V alloy," *J. Adhes.*, vol. 91, no. 7, pp. 518–537, 2014.

[44] A. G. Demir, B. Previtali, and N. Lecis, "Development of laser dimpling strategies on TiN coatings for tribological applications with a highly energetic Q-switched fibre laser," *Opt. Laser Technol.*, vol. 54, pp. 53–61, Dec. 2013.

[45] A. I. Aguilar-morales, S. Alamri, T. Kunze, and A. Fabián, "Influence of processing parameters on surface texture homogeneity using Direct Laser Interference Patterning," *Opt. Laser Technol.*, vol. 107, pp. 216–227, 2018.

[46] A. Purnama *et al.*, "Laser surface texturing of SS316L for enhanced adhesion of HUVECs,"

Surf. Eng., vol. 36, no. 12, pp. 1240–1249, 2020.